CHEMISTRY OF MATERIALS

Article

pubs.acs.org/cm

Coordination-Driven Multistep Assembly of Metal–Polyphenol Films and Capsules

Md. Arifur Rahim,[†] Hirotaka Ejima,[†,¶] Kwun Lun Cho,[†] Kristian Kempe,[†] Markus Müllner,[†] James P. Best,[†,‡] and Frank Caruso*,[†]

[†]Department of Chemical and Biomolecular Engineering, The University of Melbourne, Parkville, Victoria 3010, Australia

[‡]Laboratory for Mechanics of Materials and Nanostructures, EMPA—Swiss Federal Laboratories for Materials Science and Technology, Feuerwerkerstrasse 39, 3602 Thun, Switzerland

Supporting Information

ABSTRACT: We report the assembly of metal-polyphenol complex (MPC) films and capsules through the sequential deposition of iron(III) ions ($Fe^{(III)}$) and a natural polyphenol, tannic acid (TA), driven by metal–ligand coordination. Stable $Fe^{(III)}$/TA films and capsules were formed, indicating lateral and longitudinal cross-linking of TA by $Fe^{(III)}$ in the film structure. Quartz crystal microbalance, ultraviolet–visible (UV-vis) spectrophotometry, and X-ray photoelectron spectroscopy were carried out to quantitatively analyze the film growth. A comparison of the MPC capsules prepared through multistep assembly with those obtained through one-step deposition, as reported previously [Ejima et al., *Science* **2013**, *341*, 154–156], reveals substantial differences in the nature of complexation and in their physicochemical properties, including permeability, stiffness, and degradability. This study highlights the importance of engineering MPC films with different properties through implementing different assembly methods.

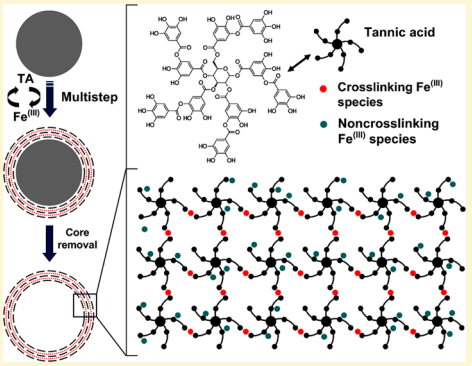

INTRODUCTION

Tannic acid (TA), homologous to hydrolyzable tannin, is a high-molecular-weight polyphenol that contains five digalloyl ester groups covalently attached to a central glucose core. TA commonly occurs in nature and exhibits antioxidant, antibacterial, antimicrobial, antimutagenic, and anticarcinogenic properties.[1−4] It is widely used for diverse industrial, pharmacological, biomedical, and food additive applications.[5−9] Furthermore, TA has unique structural properties that facilitate interactions with a variety of materials via multiple reaction pathways, including electrostatic, hydrogen bonding, and hydrophobic interactions.[10−12]

Metal chelation is a salient feature of TA (like many other polyphenols), upon which it acts as a polydentate ligand for metal ion coordination. The antioxidant ability of polyphenols is attributed to their iron chelating[13,14] and radical scavenging[15] mechanisms. Generally, the catechol or galloyl groups present in phenolic compounds provide binding sites for metal ions to chelate.[16,17] Therefore, TA, which contains galloyl groups, can form highly stable complexes with iron(III) ions ($Fe^{(III)}$), ranging from mono-type to tris-type complexes.[18] At a given pH, the nature of the complex depends mainly on the concentration of TA and its degree of ionization.

Recently, we reported a one-step approach for capsule assembly via the formation of metal-polyphenol complexes (MPCs) using TA and $Fe^{(III)}$.[19] The diverse structural and functional properties of TA, combined with its pH-dependent chelating interactions with $Fe^{(III)}$, prompted us to examine the possibility of utilizing TA and $Fe^{(III)}$ as components for the sequential (multistep) assembly[20,21] of films and capsules. We postulated that the different assembly protocols (multistep vs one-step) would yield films and capsules with different properties, which is important for the use of such materials in a range of applications.[19] Previous reports have shown that transition-metal ions and monodentate organic ligands, including Co ions and diisocyanide ligands,[22] Zn ions and bisquinoline ligands,[23] and Fe ions and resorcinol ligands,[24] can be used to form planar films. However, few studies have focused on the sequential assembly of metals and polydentate ligands.[25−27] TA has been used in alternation with a positively charged polyelectrolyte (PE) to prepare multilayered films, utilizing electrostatic interactions for film buildup.[12] TA has also been used to assemble multilayered films with neutral polymers[28] and proteins[29] via hydrogen bonding and hydrophobic interactions, respectively. A recent study reported the assembly of TA with $Fe^{(III)}$ to form multilayers;[30] however, that work involved deposition of the TA and $Fe^{(III)}$ coatings from ethanolic solutions and on polydopamine-coated substrates. These experimental differences can yield films with different characteristics. A main aim of our study was to examine differences between one-step and multistep TA/$Fe^{(III)}$ coatings;

Received: November 25, 2013
Revised: January 23, 2014
Published: February 10, 2014

hence, it was essential that the films were assembled from similar adsorption solutions (i.e., water).

In the current study, film assembly was monitored in detail by several methods (including quartz crystal microbalance (QCM), ultraviolet−visible (UV-vis) spectrophotometry, and X-ray photoelectron spectroscopy (XPS)) to elucidate the growth behavior of the MPC films. Multistep MPC capsules were obtained by templating spherical particles and by applying a subsequent template dissolution step, and were analyzed using atomic force microscopy (AFM). The nature of complexation in the multistep films was observed to be remarkably different to those prepared via one-step assembly. Furthermore, examination of the physicochemical properties of the MPC capsules, including permeability, stiffness and degradability, were found to be significantly different from those of one-step MPC capsules, thus opening opportunities to tailor the properties of MPC films/capsules for specific applications.

EXPERIMENTAL SECTION

Materials. Tannic acid (TA, ACS reagent, M_w = 1701.23 Da), iron(III) chloride hexahydrate ($FeCl_3{\cdot}6H_2O$), polyethyleneimine (PEI, M_w = 25 000 Da), fluorescein isothiocyanate (FITC), FITC-dextran with various average molecular weights (10, 70, 500, and 2000 kDa), and ethylenediamine tetraacetic acid (EDTA) were purchased from Sigma−Aldrich and used as received. Polystyrene (PS) particles (D = 3.55 ± 0.07, 10% w/v in water) were obtained from Microparticles GmbH, Germany. High-purity water (Milli-Q) with a resistivity greater than 18 MΩ cm was obtained from an in-line Millipore RiOs/Origin water purification system.

Multistep Preparation of TA/$Fe^{(III)}$ Films on Planar Substrates. Planar films were prepared on quartz crystal microbalance (QCM) resonators (silicon dioxide- and gold-coated) and quartz plates (ProSciTech, Australia) with or without a PEI precursor layer. All substrates were cleaned with piranha solution (1:3 ratio of 30% H_2O_2/98% H_2SO_4) for 2 min (QCM resonators) or 5 min (quartz plates), rinsed with copious amounts of Milli-Q water, and dried in a stream of nitrogen. [***Caution!*** *Piranha solution reacts violently with organic material and should be handled carefully.*] For in situ QCM studies, silicon dioxide-coated 5 MHz AT-cut crystals (Q-Sense AB, Västra, Frölunda, Sweden) were used and measurements were conducted using a QCM-D E4 device with four flow cells (Q-Sense AB, Västra, Frölunda, Sweden). Multistep buildup was commenced by injecting TA solutions (0.2 mg mL^{-1}, pH adjusted between 2 to 10) into the cells for 1 min. Following TA adsorption for 10 min, rinsing solutions (Milli-Q water, pH adjusted to those of the TA solutions) were injected for 1 min. Aqueous solutions of $FeCl_3{\cdot}6H_2O$ (0.05 mg mL^{-1}, pH 3.3) were then injected into the cells, 10 min allowed for adsorption, followed by injection of rinsing solutions (Milli-Q water, pH adjusted to those of the $FeCl_3{\cdot}6H_2O$ solutions) for 1 min. A flow rate of 200 μL per min was maintained for every step. The process was repeated until the desired number of deposition steps were achieved. All frequency values quoted here are those of the third overtone.

For "air-dried" QCM and UV-vis absorption measurements, cleaned substrates were primed with a PEI layer by dipping the substrates into a PEI solution (1 mg mL^{-1}, 0.5 M NaCl) for 15 min, rinsing in Milli-Q water three times, and drying under a stream of nitrogen. The PEI-coated substrates were then immersed in a TA solution (0.2 mg mL^{-1}, pH values of 3.3, 6.0, 8.0, or 10.0) for 10 min, rinsed three times with Milli-Q water, and dried under a stream of nitrogen. The pH values of the rinsing solutions (pH 3.3, 6.0, 8.0, or 10.0) were kept identical to those of the TA solution. The resulting TA-terminated substrates were then immersed in the $FeCl_3{\cdot}6H_2O$ solution for 10 min (0.05 mg mL^{-1}, pH 3.3), rinsed three times with Milli-Q water, and dried under a stream of nitrogen. The pH of the rinsing solution (pH 3.3) was kept identical to that of the $FeCl_3{\cdot}6H_2O$ solution. The last two steps were repeated until the desired number of deposition steps was achieved. QCM frequency shifts ("air-dried", gold-coated 9 MHz AT-cut crystals, Kyushu Dentsu, Japan) and UV-vis absorbance data (quartz plates) were recorded after each adsorption step.

Multistep Preparation of TA/$Fe^{(III)}$ Capsules. For capsule preparation, 50 μL of polystyrene (PS, D = 3.55 ± 0.07) particles were first washed twice with Milli-Q water. Then, 500 μL of the TA solution (0.2 mg mL^{-1}, pH 6.0, 8.0, or 10) was added to the PS particles and an adsorption time of 10 min was used. The particles were then washed three times with Milli-Q water (adjusted to pH 6.0, 8.0, or 10.0). $FeCl_3{\cdot}6H_2O$ solution was then added (0.05 mg mL^{-1}, pH 3.3) to the resulting TA-terminated PS particles and adsorbed for 10 min, followed by washing three times with Milli-Q water (adjusted to pH 3.3). In the washing steps, the particles were spun down by centrifugation (1600g, 1 min) and the supernatant was removed. The last two steps were repeated until the desired number of deposition steps was achieved. Dissolution of the PS cores was accomplished by adding THF to the particle dispersion and centrifuging for 1000g for 3 min. The obtained hollow capsules were resuspended in 500 μL of Milli-Q water.

Permeability Experiments. Multistep capsule suspensions, $(TA/Fe^{(III)})_{4.5}$ (~4×10^7 capsules mL^{-1}), were mixed with an equal volume of FITC-dextran solution (2 mg mL^{-1}). Confocal laser scanning microscopy (CLSM) images of the capsules were obtained within 10 min. One hundred (100) capsules were examined for each FITC-dextran M_w. The capsules with dark interiors were considered to be impermeable and those with similar inner and outer environments were considered to be permeable.

Disassembly Experiments. Multistep capsule suspensions, $(TA/Fe^{(III)})_{4.5}$ (~4×10^7 capsules mL^{-1}), in 100 mM EDTA (pH 7.4), 50 mM Gly-HCl (pH 3.0), 50 mM Gly-HCl (pH 2.0), and 1 M HCl were incubated in a thermostatted shaker bath at 37 °C for the required time. The suspensions were diluted with Milli-Q water and flow cytometry assays were performed to count the number of capsules. Differential interference contrast (DIC) microscopy images were taken on an inverted Olympus Model IX71 microscope equipped with a DIC slider (U-DICT, Olympus) with a 60× objective lens.

Capsule Deformation Experiments. Details of the AFM force spectroscopy measurements can be found elsewhere.[19] In brief, the measurements were performed in Milli-Q water using colloidal probe (D = 35 μm)-modified cantilever tips (spring constant = 52.5 mN m^{-1}). To fabricate the modified cantilevers, tipless cantilevers were first calibrated on a cleaned glass substrate to determine the inverse optical lever sensitivity (InvOLS), and the spring constant was determined using the thermal noise method. A spherical glass bead (Polysciences) was attached to the cantilever using an epoxy resin (Selleys Araldite Super Strength, Selleys) via careful micromanipulation using an atomic force microscopy (AFM) system and associated optics. The probe was then allowed to dry overnight. Glass slides and cantilevers were cleaned with isopropanol, water, and plasma treatment to remove any contaminant material. PEI-coated glass slides were used to immobilize the capsules prior to the measurements. Force−distance curves were obtained by optically positioning the probe over individual multistep capsules ($(TA/Fe^{(III)})_{4.5}$) and an approach-retract cycle was initiated. The temperature was controlled within 19−21 °C during the force measurements (JPK BioCell). Collected force spectra were analyzed using JPK data processing software. A baseline was first subtracted from the noncontact z-range of the force-displacement data and a probe/surface contact point was assigned. After subtracting the effect of the cantilever bending, force-deformation (F-δ) data were obtained. The E_Y of the spherical capsules could be estimated using the Reissner model for thin-walled spherical shells. Using the Reissner equation with a wall thickness (h) of 10.2 nm, a Poisson's ratio (ν) of 0.5, and an effective probe radius (R_{eff}) of 1.60 μm, the E_Y of the multistep capsules was determined. Only the deformation data over the capsule shell thickness was used. The obtained results were confirmed with measurements using a stiffer cantilever (spring constant = 90.2 mN m^{-1}, probe diameter = 32.4 μm).

Instrumentation. For the mass adsorption studies in air, a QCM device (Hewlett−Packard) with ~9 MHz electrodes (resonance frequency) was used. UV-vis absorption spectra were recorded on a

Varian Cary Model 4000 UV-vis spectrophotometer. Zeta-potential measurements were performed on a Malvern Nano-ZS zetasizer (Malvern Instruments, U.K.) at room temperature. For AFM measurements (topographic imaging), capsule dispersions were cast and air-dried on clean glass slides and mounted on a NanoWizard II AFM (JPK Instruments, Berlin, Germany). Images were taken in tapping mode with MikroMasch silicon cantilevers (NSC15/AIBS, spring constant = 46 N m^{-1}) with a resonant frequency of 325 kHz. Force spectroscopy measurements were also performed on the same instrument. X-ray photoelectron spectroscopy (XPS) spectra were obtained using a VG ESCALAB 220i-XL spectrometer equipped with a monochromated Al Kα X-ray source with an emitted photon energy of 1486.6 eV at 10 kV and 12 mA. Measurements were processed at a step size of either 1 eV (wide scans) or 0.1 eV (region scans). Film samples (on quartz) were screwed down to Al holders and samples were measured in the analysis chamber at a typical operating pressure of ~1 × 10^{-9} Pa.

RESULTS AND DISCUSSION

QCM experiments were performed to follow the multistep growth of the TA and $Fe^{(III)}$ films. Sequential assembly was conducted under different pH conditions of the TA solution, as displayed in Figure 1. The pH of the $Fe^{(III)}$ solution was kept

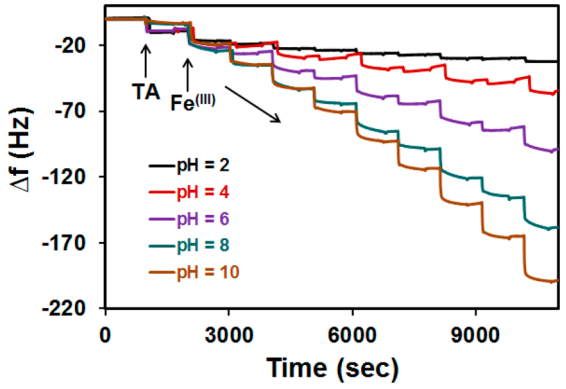

Figure 1. Metal-polyphenol complex (MPC) film growth via multistep assembly (10 steps, $(TA/Fe^{(III)})_5$) at different pH values of the TA solution, monitored in situ using a QCM (5 MHz resonators).

constant at 3.3. By alternately depositing the TA and $Fe^{(III)}$, with intermediate rinsing steps, the QCM resonance frequency gradually decreased, indicating the successful deposition of each component. Film assembly was found to be pH-dependent, with the deposited amount increasing with increasing pH (after the first TA layer). However, the first TA layer showed a reverse trend due to the enhanced electrostatic repulsion between the substrate (silica) and TA (acid dissociation constant, $pK_a \approx 8.5$, see later discussion) with higher pH values.

QCM measurements in the "dry state" (i.e., in air) were also performed. The pH values of the TA solution were selected to be 3.3 and 6.0, while the pH of $Fe^{(III)}$ solution was kept at 3.3. The pristine pH for $Fe^{(III)}$ solution (0.05 mg mL^{-1}) is 3.3, and above pH 4.3, $Fe^{(III)}$ forms insoluble hydroxide species (solubility product, K_{sp} for $Fe(OH)_3$ is ~6 × 10^{-39}).[31] For this reason, the pH of the $Fe^{(III)}$ solution was not altered. The pH values of the rinsing solutions were adjusted accordingly (see Experimental Section for details). Moreover, the substrate was made positively charged by a polyethyleneimine (PEI) precursor layer for better adhesion of the first TA layer. Under these set conditions, in-air QCM measurements were performed after each deposition step, as shown in Figure 2. Consistent with the in situ (in liquid) QCM results (Figure 1),

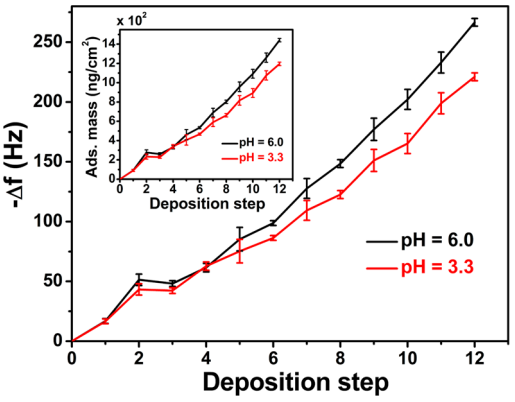

Figure 2. QCM frequency shift (9 MHz resonators) with each deposition step in the "dry state" at a pH of 3.3 or 6.0 for the TA solution, and the corresponding mass adsorbed (inset) in each step. Adsorbed mass values (inset, *y*-axis) range from 0 to 1550 ng/cm^2.

the frequency decreased with each deposition step at both pH values, indicating gradual mass adsorption, but not as significant as those observed in the in situ experiments, suggesting that film hydration contributes to the in situ film buildup. Further, the differences in frequency shifts at pH 3.3 and 6.0 in the "dry state" measurements were less pronounced than in the in situ growth of the films. After the deposition of the first layer of $Fe^{(III)}$, the frequency increased slightly, indicating desorption of some materials. This can be explained by the fact that in the presence of $Fe^{(III)}$ ions, the apparent pK_a (i.e., the degree of ionization) of the underlying TA and PEI layer varied in such a way that the electrostatic attraction between TA and PEI became weaker. As a result, some preadsorbed TA detached from the surface. However, the adsorbed mass was larger than the mass desorbed by the $Fe^{(III)}$ step, resulting in a net increase in frequency. The remaining steps showed a steady and linear film growth. The mass deposited for each layer, calculated from the frequency change, is presented in the inset of Figure 2. For 10 steps of $TA/Fe^{(III)}$ deposition, the adsorbed mass ratio of TA to $Fe^{(III)}$ was found to be ~1:1.1 and ~1:1.2 at pH 3.3 and 6.0, respectively (assuming a M_w of 1701.19 Da for TA). Although the chemical formula of TA is generally considered to be that of decagalloyl glucose ($C_{76}H_{52}O_{46}$), it exists as a mixture of polygalloyl glucose molecules with different degrees of esterification.[32] Hence, the exact molecular weight of TA is uncertain.

To further investigate film formation at pH 3.3 and 6.0, UV-vis absorption spectrophotometry was used to follow the multistep assembly (Figure 3). Prior to film assembly, the absorbance of the TA in solution as a function of pH was measured to determine its pK_a value (see Figure S1 in the Supporting Information). The reported pK_a of TA varies significantly, from 2.5 to 8.5.[12,28] This discrepancy is probably caused by the use of different tannin sources. At pH 4, the UV-vis absorption spectrum of TA in solution exhibited two peaks, centered at ~225 nm and ~274 nm. These peaks can be assigned to the neutral (i.e., protonated) form of TA.[12,33] However, both peaks shifted slightly to longer wavelengths with increasing pH. At pH 7 and 8, a concomitant shoulder appears at ~325 nm. With further elevation in pH, a clear peak emerged at ~325 nm and its intensity reaches a maximum at pH 10. The absorption peak at ~325 nm corresponds to the phenolate form of TA resulting from ionization of the phenolic hydroxyl groups in basic solution.[12,33] To determine the pK_a of TA, the

dx.doi.org/10.1021/cm403903m | *Chem. Mater.* 2014, 26, 1645−1653

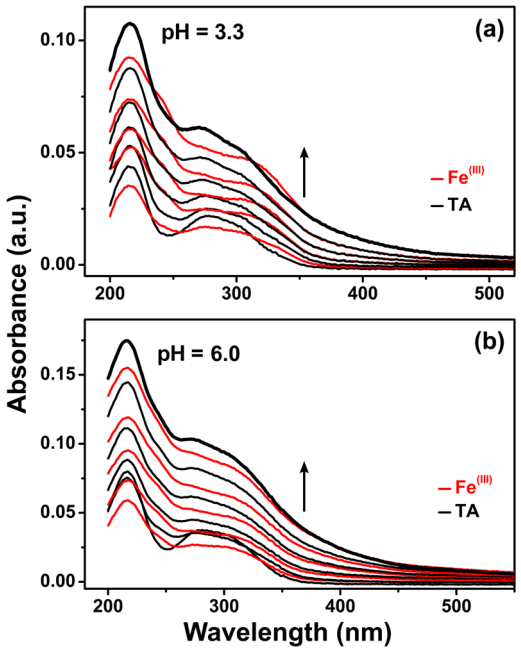

Figure 3. UV−vis absorption spectra of MPC films (up to 11 deposition steps) assembled at (a) pH 3.3 and (b) pH 6.0. The arrows indicate an increasing number of deposition steps.

ratio of peak intensities at 325 and 274 nm (denoted by A_{325}/A_{274}) at different pH were calculated and plotted in Figure S1 in the Supporting Information (inset). The calculated ratio showed a sharp increase between pH 8 and pH 10. Similar TA ionization behavior was observed earlier by Erel-Unal and Sukhshivili.[28] Assuming a negligible difference in the extinction coefficients of neutral and ionized forms of TA (at 274 nm and at 325 nm, respectively), the pK_a was calculated from the equivalence point on the curve, giving an estimated value of ∼8.5, which agrees well with other reports.[11,28]

Analogous to the behavior of TA in solution, the absorbance of the films can be attributed to (i) the neutral (i.e., protonated) form of TA showing a peak at ∼215 nm and a broadened peak at ∼270 nm; and (ii) the phenolate (i.e., deprotonated) form of TA showing a shoulder at ∼305 nm. However, in the $Fe^{(III)}$ deposition step, the latter peak shifted slightly to longer wavelengths, suggesting conjugation between $Fe^{(III)}$ and the deprotonated form of TA. The degree of ionization of TA at both pH values appeared to be much higher in the films than in solution, and oscillated between ∼40% and ∼45% (calculated from the ratio of absorbance at 305 and 270 nm) when TA and $Fe^{(III)}$ were the adsorbing species, respectively. Evidently, the presence of $Fe^{(III)}$ in the film decreased the apparent pK_a of TA in the film and shifted the degree of ionization. This observation is consistent with what is generally observed in polyelectrolyte multilayer films, and can be described by the internal charge adjustment of the components in the film.[34] It is also noted from Figure 3 that, after a certain number of deposition steps, the absorbance values generally increased following $Fe^{(III)}$ adsorption. This behavior was more pronounced in films assembled at pH 6.0 compared with those prepared at pH 3.3. There are three possible explanations for the observed phenomenon: (i) a hyperchromic shift due to changes in the nature of TA and $Fe^{(III)}$ conjugation; (ii) a change in refractive index of the film; and/or (iii) an additive effect from the absorbance of different $Fe^{(III)}$ species in the film. Since $Fe^{(III)}$ in solution showed a broad spectrum with an absorption maxima at ∼295 nm (see Figure S2 in the Supporting Information), the additive effect is likely to be the major factor. However, this peak was not well-resolved in the film structure, because of overlap with TA peaks. UV-vis absorption spectra of films assembled from TA solutions at basic pH values (pH 8.0 and pH 10.0) are presented in Figure S3 in the Supporting Information. We note that, at these pH values, polyphenolic (TA) polymerization occurs.[35]

Recently, we reported a one-step assembly technique for the preparation of capsules (denoted as "one-step" MPC capsules) based on the same MPC system (TA and $Fe^{(III)}$).[19] Visible inspection of capsules prepared by one-step and multistep assembly revealed a remarkable color difference (Figure S4 in the Supporting Information). The color of the one-step MPC capsules was blue-black with a well-resolved (but broad) ligand-to-metal charge-transfer band (LMCT; here ligand refers to TA) in the UV-vis absorption spectrum at ∼570 nm (Figure S5 in the Supporting Information). In contrast, the reported multistep system herein shows a faint yellow-brownish color with no resolvable LMCT band. The LMCT band of the one-step MPC system can be explained by the formation of tris-type complexes commonly observed in solution systems.[18,36] The metal-to-ligand ratio, along with the pH and final concentration of the solution, were found to be the major factors governing the formation of different types of metal-polyphenol complexes in solution.[18,36,37]

The absence of both a well-resolved LMCT band and the blue-black color in the multistep-assembled films can be visualized by the aforementioned low ligand (when $Fe^{(III)}$ species adsorb) and high ligand (when TA adsorbs) concentrations and the corresponding pH values. Switching between these two concentrations regulates the molecular interactions between TA and $Fe^{(III)}$ during film formation, as depicted in Scheme 1. When the $Fe^{(III)}$ species deposit on a preadsorbed TA layer (low ligand concentration, pH 3.3), $Fe^{(III)}$ occupies the available binding sites (deprotonated galloyl groups) provided by TA. Hence, the formation of complexes with a low metal-to-ligand (TA) ratio is unlikely. Previous studies on $Fe^{(III)}$ and gallic acid (a major constituent of TA) suggested a 1:1 complex formation in acidic pH[38] and the absence of a LMCT band (gallic acid as the ligand here) at low ligand concentration.[39] However, lateral cross-linking (top left panel, Scheme 1) might occur between two galloyl groups from different TA molecules. On the other hand, when TA adsorbs on preadsorbed $Fe^{(III)}$ (top right panel, Scheme 1), TA is only able to interact with $Fe^{(III)}$ that is bound to the top of the underlying TA layer. This creates longitudinal cross-linking where $Fe^{(III)}$ is sandwiched between two galloyl groups from lower and upper TA molecules. Here, because of steric hindrance (indicated by a green cross over the arrow), even the formation of a local tris-type complex is unlikely. A similar situation can be presented in analogous solution systems (bottom panel, Scheme 1), where the main difference is that TA is mobile at the high ligand concentration (right bottom panel, Scheme 1) and can form tris-type complexes (indicated by a violet sphere) locally or as a whole, depending on the pH and concentration of the solution. UV−vis absorption spectra of TA-$Fe^{(III)}$ complexes at low ligand concentrations in solution (pH 3.3) (Figure S6 in the Supporting Information) further support this assumption: no blue-black color or well-resolved

dx.doi.org/10.1021/cm403903m | *Chem. Mater.* 2014, 26, 1645−1653

Scheme 1. Illustration Showing the Different Interaction Modes of TA and $Fe^{(III)}$ at Low and High Ligand Concentrations

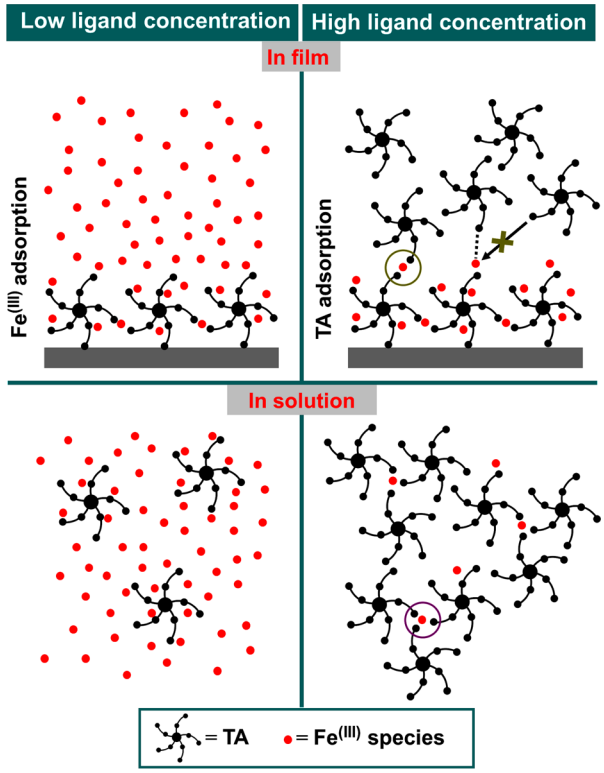

LMCT band appeared, even if the $Fe^{(III)}$:TA ratio was as high as 1:0.05.

XPS was performed to determine the stoichiometry of TA and $Fe^{(III)}$ in the films. As displayed in Figure 4, C 1s, O 1s, N 1s, and Fe 2p peaks were detected in the survey spectra, and this is in agreement with the film compositions at both pH values. From the C 1s core-level photoelectron spectrum, the binding energy (BE) was observed to be ~285 eV and can be attributed to the presence of hydrocarbons in TA and PEI.[40] For both types of films (pH 3.3 and 6.0), the Fe $2p_{3/2}$ signal showed a main peak at ~711 eV with a 2p peak separation of ~12−14 eV, consistent with the presence of $Fe^{(III)}$ species.[40] From the deconvoluted O 1s spectra (Figure S7 in the Supporting Information), peaks appearing at ~531.2 eV and ~533 eV can be assigned to Fe−O and Fe−OH species, respectively. Fe−O arises from the coordination between TA and $Fe^{(III)}$, as reported previously.[40−42] By integration of the elemental peaks with respect to their individual sensitivity factors, the atomic compositions of the films were calculated: TA:$Fe^{(III)}$ ratios of ~1:2.5 and ~1:3 were obtained for films assembled at pH 3.3 and 6.0, respectively. XPS spectra for the pH 6.0 film are displayed in Figure S8 in the Supporting Information. This result further confirmed the absence of tris-type TA-$Fe^{(III)}$ (TA:Fe = 3:1) complexes in the film.

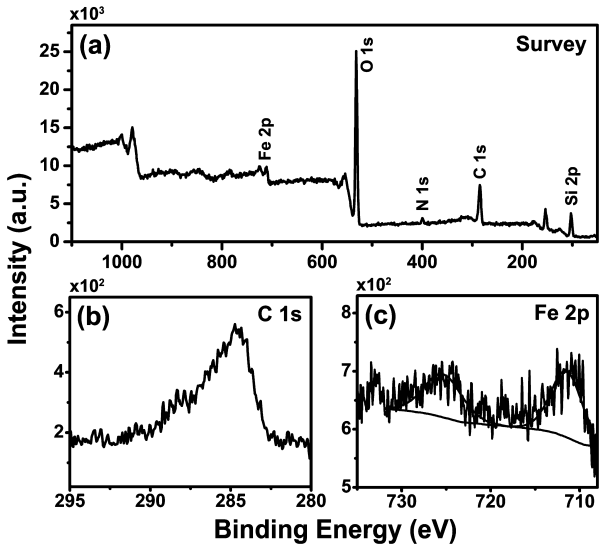

Figure 4. XPS spectra of a MPC film ($(TA/Fe^{(III)})_5$) assembled at pH 3.3: (a) survey spectrum, (b) C 1s core-level spectrum, and (c) Fe 2p core-level spectrum.

The experimental observations presented above contribute to the film growth mechanism shown in Scheme 2. Confirmation by XPS, and the absence of a LMCT band, suggests that tris-type complexes with a molar ratio of ~3:1 (TA:$Fe^{(III)}$) are not the dominant species in the film. The adsorbed mass ratio of TA and $Fe^{(III)}$ from the QCM results is ~1:1. According to these results, the adsorbing $Fe^{(III)}$ species bound to TA in the film might range from a combination of monomeric, dimeric, and trimeric ferric aqua hydroxo complexes.[43,44] Moreover, outer shell hydration[45] (second hydration sphere, not shown) might occur due to hydrogen bonding interaction of the water (H_2O) molecules coordinated to $Fe^{(III)}$ ions, which contributes significantly to the mass of the films. Since ferric hydroxo dimers show an absorption maximum at ~335 nm,[46] the existence of the hydroxo complexes in this system is confirmed by the broad absorption spectrum of $Fe^{(III)}$ in aqueous solution (deconvoluted spectra; see Figure S2 in the Supporting Information). Moreover, the concentration (0.05 mg mL^{-1}) and pH (3.3) of the $Fe^{(III)}$ solution (used in this study) further supports the existence of multinuclear $Fe^{(III)}$ entities.[38,44] Hence, the presence of such species in the films can be justified. However, for the cross-linking $Fe^{(III)}$ species, the coordinated H_2O should be largely substituted by TA ligands compared to the noncross-linking $Fe^{(III)}$ species. In addition, the formation and stability of the hollow microcapsules (see Figures 5 and 6) demonstrate excellent lateral and longitudinal cross-linking by $Fe^{(III)}$ species. Following successful film assembly on planar substrates, microcapsules were prepared using spherical sacrificial polystyrene (PS) templates (D = 3.6 μm). These templates were removed by exposure to tetrahydrofuran (THF).[47−49] Optical micrographs show the successful formation of monodispersed capsules with no apparent aggregation (Figure 5a, b). Two types of capsules were prepared (using either 9 or 13 deposition steps) at pH 6.0 for the TA solution and are denoted as $(TA/Fe^{(III)})_n$, where n = 4.5 or 6.5, respectively. Figures 5c and 5d represent the AFM images of air-dried capsules of $(TA/Fe^{(III)})_{4.5}$ and $(TA/Fe^{(III)})_{6.5}$, respectively. The average shell thickness was determined to be 10.2 ± 0.5 nm for $(TA/Fe^{(III)})_{4.5}$ and 14.1 ± 0.2 nm for $(TA/Fe^{(III)})_{6.5}$. The average $(TA/Fe^{(III)})_1$ thicknesses in both $(TA/Fe^{(III)})_{4.5}$ and $(TA/Fe^{(III)})_{6.5}$ films were found to be in good agreement with each other (~2.2 nm). Moreover, the difference between the total shell thickness of $(TA/Fe^{(III)})_{6.5}$ and $(TA/Fe^{(III)})_{4.5}$ capsules gave an average $(TA/Fe^{(III)})_1$ thickness of ~2 nm. This value is slightly lower than the 2.7 nm/bilayer thickness reported for $(Fe^{(III)}/TA)_{10}$ films assembled from ethanolic solutions.[30] The reported

dx.doi.org/10.1021/cm403903m | Chem. Mater. 2014, 26, 1645−1653

Scheme 2. Illustration of the Proposed Growth Mechanism for Multistep Assembly of MPC Films[a] (Molecular Structure of TA (Right Panel), and Small Black Dots Represent the Gallol Groups)

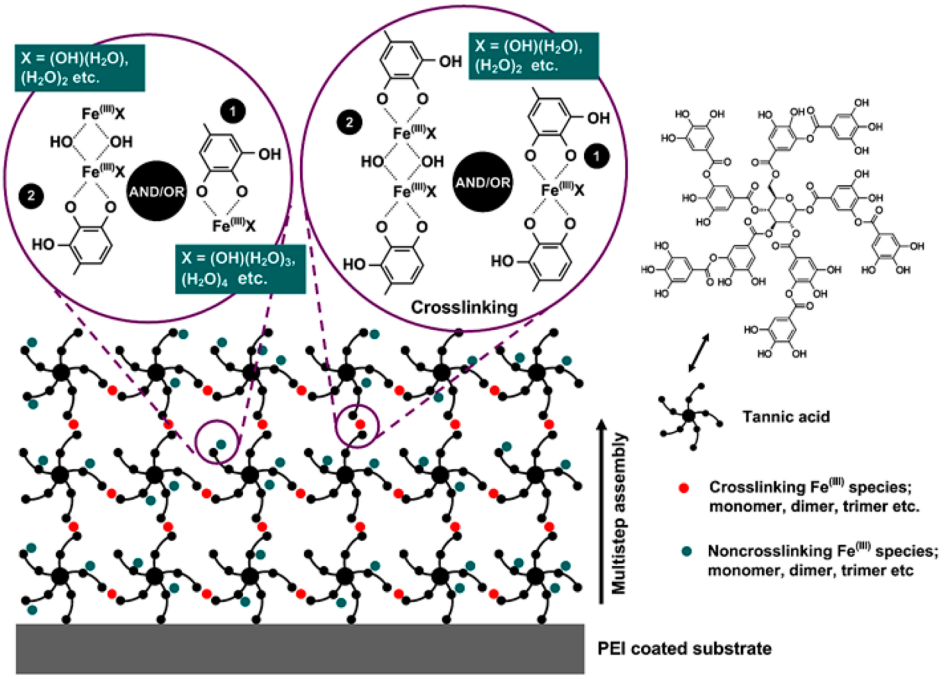

[a]Crosslinking and noncross-linking $Fe^{(III)}$ species are shown in different colors for clarity.

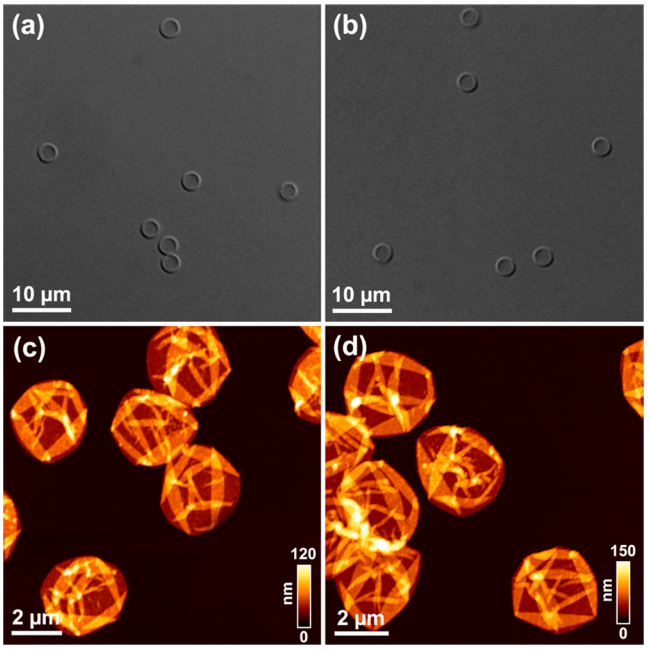

Figure 5. (a) Optical microscopy image of $(TA/Fe^{(III)})_{4.5}$ capsules; (b) optical microscopy image of $(TA/Fe^{(III)})_{6.5}$ capsules; (c) AFM image of $(TA/Fe^{(III)})_{4.5}$ capsules; and (d) AFM image of $(TA/Fe^{(III)})_{6.5}$ capsules.

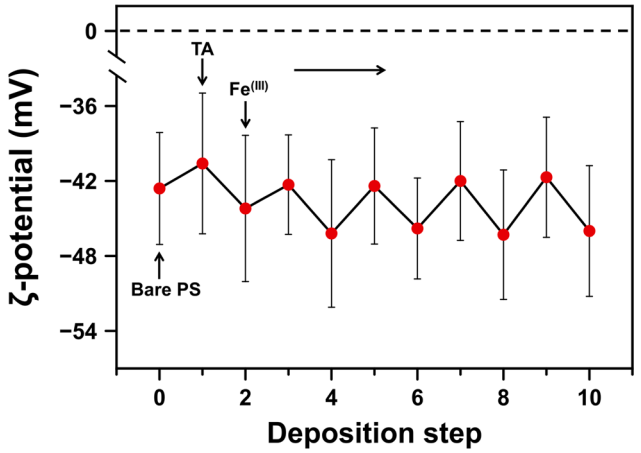

Figure 6. Zeta (ζ)-potential measurements for the growth of $(TA/Fe^{(III)})_5$ films on polystyrene (PS) particles.

average molecular diameter of TA varies from 1.7 to 3 nm.[12,50,51] In addition, no appreciable shrinking or swelling of the capsules was observed after template removal.

Microelectrophoresis was used to examine zeta (ζ)-potentials of the $TA/Fe^{(III)}$ films during growth (Figure 6). Bare PS particles showed a ζ-potential of −43 mV. Next, the TA was adsorbed and the ζ value was found to be −41 mV. However, the successive steps of $Fe^{(III)}$ did not result in charge reversal of the particle and the ζ-potential oscillated around −42 mV. This implies that most of the $Fe^{(III)}$ adsorbed inside the film structure and the amount retained on the surface was not sufficient enough to overcome the negative potential created by TA. Moreover, UV−vis absorbance spectra for the planar film suggested an increased ionization of TA due to the adsorption of $Fe^{(III)}$, which may shift the ζ-potential value to more negative, and may explain the slight oscillation in negative ζ-potential after the alternate deposition steps. For the MPC films, where very small molecules such as TA and metal ions are assembled via complexation through coordination bonds, charge compensation and overcompensation may not play a significant role for multistep growth. This is consistent with an earlier report,[52] which shows the absence of complete charge

dx.doi.org/10.1021/cm403903m | Chem. Mater. 2014, 26, 1645−1653

reversal for terbium ion/polystyrene sufonate ($Tb^{(III)}$/PSS) multilayers.

We also investigated several macroscopic properties of the multistep system and compared the results with those of our previously reported one-step system.[19] For comparison, we chose equivalent shell thicknesses of capsules for both systems. The reported mean shell thickness for one-step capsules was ~10 nm; hence, we performed the experiments with the multistep capsules $(TA/Fe^{(III)})_{4.5}$, which exhibit a shell thickness of ~10 nm. First, the permeability of the multistep system was investigated. As shown in Figure 7, multistep

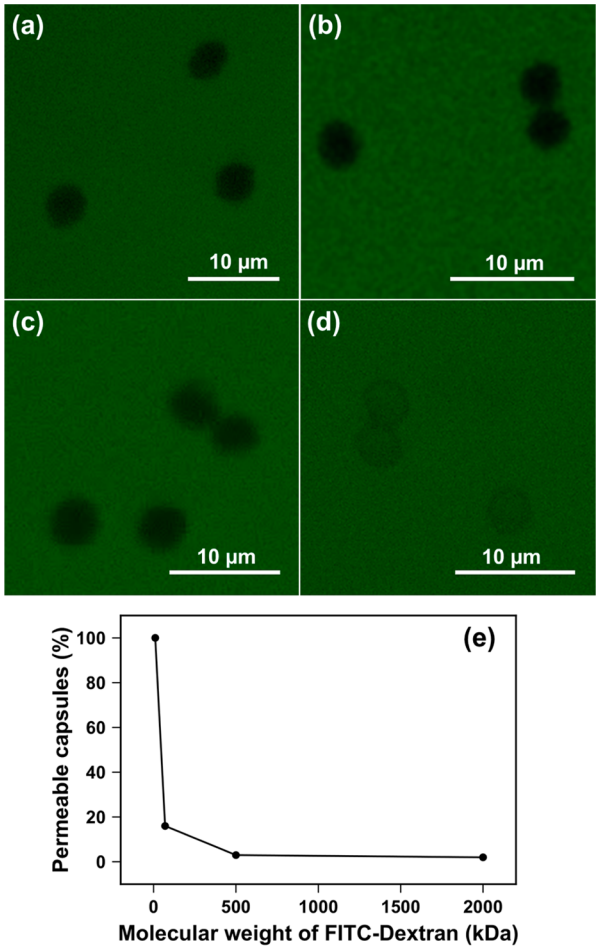

Figure 7. CLSM images of $(TA/Fe^{(III)})_{4.5}$ multistep capsules incubated with FITC-Dextran: (a) 2000 kDa, (b) 500 kDa, (c) 70 kDa, and (d) 10 kDa. (e) Plot of the percentage of permeable capsules versus different molecular weights of FITC-dextran.

capsules were completely impermeable to 500 kDa FITC-Dextran and over 80% of the capsules were impermeable to 70 kDa FITC-Dextran. However, they were fully permeable to 10 kDa FITC-Dextran. In contrast, the one-step system was reported to be semipermeable to 70 kDa and 500 kDa FITC-Dextran (~40% and ~30%, respectively), and impermeable to 2000 kDa FITC-Dextran.[19] These results indicate that the multistep MPC films have a smaller mesh size than the one-step films.

Next, we compared the shell stiffness of the multistep capsules to the one-step capsules previously reported.[19] AFM force measurements using a colloidal indenter were performed to determine the Young's modulus (E_Y) of the multistep capsules. Figure 8 shows four separate force−deformation curves for the $(TA/Fe^{(III)})_{4.5}$ multistep capsules and curves for

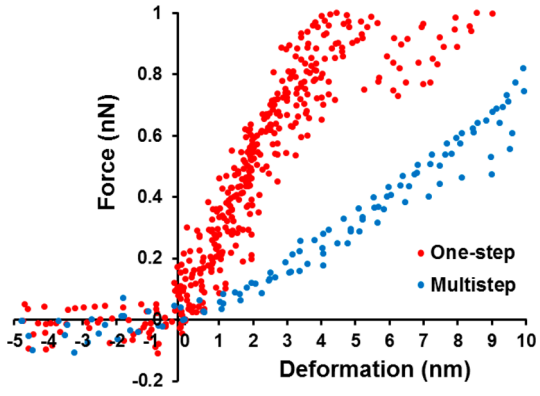

Figure 8. Representative force−deformation ($F-\delta$) curves for the small deformation regime of $(TA/Fe^{(III)})_{4.5}$ multistep capsules (blue). Force-deformation curves for one-step capsules (red) are also presented for comparison. Data (one-step capsules) taken from ref 19. Copyright 2013, American Association for the Advancement of Science. Four separate $F-\delta$ curves are shown for both systems.

the one-step capsules[19] are also presented for comparison. The variation in slope for the two systems implies that the multistep capsules are significantly more compliant than the one-step capsules, as the indenter geometry was constant between both measurements. The E_Y for the multistep capsules was calculated to be 420 ± 30 MPa, which is ~40% of the E_Y reported for the one-step capsules (1.0 ± 0.2 GPa).[19] This result also suggests that tris-type complexes ($TA:Fe^{(III)} \approx 3:1$), being a dominant species, might give rise to the higher stiffness of such films in the one-step system. It is noteworthy to mention that the E_Y observed for the multistep capsules sits in the intermediate range reported for layer-by-layer (LbL) polyelectrolyte capsule shells (10−1000 MPa) interrogated using equivalent methodologies.[53]

Finally, the degradability of the multistep capsules, $(TA/Fe^{(III)})_{4.5}$, was examined. Interestingly, multistep capsules were found to be nondegradable when incubated in pH 2, pH 3, and EDTA solutions for at least three days. Furthermore, their colloidal stability was lost in those solutions and the capsules aggregated (Figure S9 in the Supporting Information). However, multistep capsules were degradable in 1 M HCl solution. In contrast, one-step capsules showed rapid degradation under the same conditions (pH 2, pH 3, or EDTA solutions).[19] The reason for this enhanced stability of the multistep system is not clear; however, it may be possible that the $Fe^{(III)}$ ions induce intermolecular oxidative C−C coupling[54,55] of TA molecules in the film. These covalent cross-links might contribute to enhance the stability of the films. Further studies are currently underway to examine the cross-linking in the films.

CONCLUSION

Metal-polyphenol film formation utilizing coordination bonding between tannic acid (TA) and the trivalent iron cation ($Fe^{(III)}$) through multistep assembly has been explored. A growth mechanism of the coordination-driven film buildup was postulated, considering the stoichiometry of TA and $Fe^{(III)}$ inside the film and the interchange between low and high ligand concentrations. The growth behavior and nature of

dx.doi.org/10.1021/cm403903m | Chem. Mater. 2014, 26, 1645−1653

complexation of the presented multistep MPC film deviate in several aspects from one-step MPC films;[19] this provides insights into how film formation for the MPC systems can be tailored by exploiting different assembly protocols (one-step or multistep). In addition, we have also demonstrated that the properties exhibited by multistep MPC capsules differ to those of one-step MPC capsules. Since MPC systems possess useful bioactive features due to the presence of natural polyphenols, they can be useful for a range of applications including drug delivery, biosensing, and bioimaging. A judicious choice can be made between the two protocols, one-step or multistep, considering their relative nature of complexation and properties for case-specific applications.

■ ASSOCIATED CONTENT

Supporting Information

Additional experimental data containing UV-vis absorption spectra of TA solution at different pH values, UV-vis absorption spectrum of an aqueous solution of $FeCl_3 \cdot 6H_2O$, UV-vis absorption spectra of MPC films assembled at pH 8.0 and 10.0, UV-vis absorption spectra of one-step MPC capsules showing the LMCT band, UV-vis absorption spectra of solutions containing different mixing molar ratios of $Fe^{(III)}$ and TA at pH 3.3, photographs showing the color difference of one-step and multistep MPC capsules, deconvoluted XPS spectra of O 1s for MPC films assembled at pH 3.3, XPS spectra of multistep MPC films assembled at pH 6.0, and optical microscopy images of aggregated multistep capsules in different solutions. This material is available free of charge via the Internet at http://pubs.acs.org.

■ AUTHOR INFORMATION

Corresponding Author

*Tel.: +61 3 8344 3461. Fax: +61 3 8344 4153. E-mail: fcaruso@unimelb.edu.au.

Present Address

[¶]Institute of Industrial Science, The University of Tokyo, 4-6-1 Komaba, Meguro-ku, Tokyo, Japan.

Author Contributions

The manuscript was written through contributions of all authors. All authors have given approval to the final version of the manuscript. The authors declare no competing financial interest.

Notes

The authors declare no competing financial interest.

■ ACKNOWLEDGMENTS

This research was supported by the Australian Research Council under the Australian Laureate Fellowship (FL120100030, F.C.) scheme. H.E. thanks the Japan Society for the Promotion of Science (JSPS) for a postdoctoral fellowship. K.K. is grateful to the Alexander von Humboldt-foundation for a Feodor-Lynen fellowship. M.M. thanks the University of Melbourne for a McKenzie postdoctoral fellowship. J.P.B. would like to acknowledge funding from the EMPA Postdoc program cofunded by FP7:Marie Curie Actions. K.L.C thanks the Science and Industry Endowment Fund and CSIRO for a John Stocker Postdoctoral Fellowship.

■ ABBREVIATIONS

TA = tannic acid; MPC = metal-polyphenol complex; AFM = atomic force microscopy; QCM = quartz crystal microbalance; XPS = X-ray photoelectron spectroscopy; LMCT = ligand-to-metal charge transfer.

■ REFERENCES

(1) Kim, T. J.; Silva, J. L.; Kim, M. K.; Jung, Y. S. *Food Chem.* **2010**, *118*, 740−746.
(2) Chung, K. T.; Lu, Z.; Chou, M. W. *Food Chem. Toxicol.* **1998**, *36*, 1053−1060.
(3) Mukhtar, H.; Das, M.; Khan, W. A.; Wang, Z. Y.; Bik, D. P.; Bickers, D. R. *Cancer Res.* **1988**, *48*, 2361−2365.
(4) Hayatsu, H.; Arimoto, S.; Negishi, T. *Mutat. Res.* **1988**, *202*, 429−446.
(5) Chung, K. T.; Wong, T. Y.; Wei, C. I.; Huang, Y. W.; Lin, Y. *Crit. Rev. Food Sci. Nutr.* **1998**, *38*, 421−464.
(6) Tondi, G.; Fierro, V.; Pizzi, A.; Celzard, A. *Carbon* **2009**, *47*, 1480−1492.
(7) Kozlovskaya, V.; Harbaugh, S.; Drachuk, I.; Shchepelina, O.; Kelley-Loughnane, N.; Stone, M.; Tsukruk, V. V. *Soft Matter* **2011**, *7*, 2364−2372.
(8) Kim, B. S.; Lee, H. I.; Min, Y.; Poon, Z.; Hammond, P. T. *Chem. Commun.* **2009**, *28*, 4194−4196.
(9) Shutava, T. G.; Balkundi, S. S.; Vangala, P.; Steffan, J. J.; Bigelow, R. L.; Cardelli, J. A.; O'Neal, D. P.; Lvov, Y. M. *ACS Nano* **2009**, *3*, 1877−1885.
(10) Oh, H. I.; Hoff, J. E.; Armstrong, G. S.; Haff, L. A. *J. Agr. Food Chem.* **1980**, *28*, 394−398.
(11) Costa, E.; Coelho, M.; Ilharco, L. M.; Aguiar-Ricardo, A.; Hammond, P. T. *Macromolecules* **2011**, *44*, 612−621.
(12) Shutava, T.; Prouty, M.; Kommireddy, D.; Lvov, Y. *Macromolecules* **2005**, *38*, 2850−2858.
(13) Sestili, P.; Diamantini, G.; Bedini, A.; Cerioni, L.; Tommasini, I.; Tarzia, G.; Cantoni, O. *Biochem. J.* **2002**, *364*, 121−128.
(14) Perron, N. R.; Hodges, J. N.; Jenkins, M.; Brumaghim, J. L. *Inorg. Chem.* **2008**, *47*, 6153−6161.
(15) Pietta, P.-G. *J. Nat. Prod.* **2000**, *63*, 1035−1042.
(16) Khokhar, S.; Apenten, R. K. O. *Food Chem.* **2003**, *81*, 133−140.
(17) Andjelkovic, M.; Camp, J. V; Meulenaer, B. D; Depaemelaere, G.; Socaciu, C.; Verloo, M.; Verhe, R. *Food Chem.* **2006**, *98*, 23−31.
(18) Perron, N. R.; Brumaghim, J. L. *Cell Biochem. Biophys.* **2009**, *53*, 75−100.
(19) Ejima, H.; Richardson, J. J.; Liang, K.; Best, J. P.; van Koeverden, M. P.; Such, G. K.; Cui, J.; Caruso, F. *Science* **2013**, *341*, 154−156.
(20) Skorbab, E. V.; Andreeva, D. V. *Polym. Chem.* **2013**, *4*, 4834−4845.
(21) Ariga, K.; Ji1, Q.; Hill, J. P.; Bando, Y.; Aono, M. *NPG Asia Mater.* **2012**, *4*, e17.
(22) Ansell, M. A.; Zeppenfeld, A. C.; Yoshimoto, K.; Cogan, E. B.; Page, C. J. *Chem. Mater.* **1996**, *8*, 591−594.
(23) Thomsen, D. L.; Phely-Bobin, T.; Papadimitrakopoulos, F. *J. Am. Chem. Soc.* **1998**, *120*, 6177−6178.
(24) Liu, M.; Kira, A.; Nakahara, H. *Langmuir* **1997**, *13*, 779−783.
(25) Kim, J.; Wang, H. C.; Kumar, J.; Tripathy, S. K.; Chittibabu, K. G.; Cazeca, M. J.; Kim, W. *Chem. Mater.* **1999**, *11*, 2250−2256.
(26) Maier, A.; Tieke, B. *J. Phys. Chem. B* **2012**, *116*, 925−934.
(27) Wanunu, M.; Vaskevich, A.; Cohen, S. R.; Cohen, H.; Arad-Yellin, R.; Shanzer, A.; Rubinstein, I. *J. Am. Chem. Soc.* **2005**, *127*, 17877−17887.
(28) Erel-Unal, I.; Sukhishvili, S. A. *Macromolecules* **2008**, *41*, 3962−3970.
(29) Shukla, A.; Fang, J. C.; Puranam, S.; Jensen, F. R.; Hammond, P. T. *Adv. Mater.* **2012**, *24*, 492−496.
(30) Kim, S.; Kim, D. S.; Kang, S. M. *Chem. Asian J.* **2014**, *9*, 63−66.
(31) Ebbing, D. D. *General Chemistry*, 5th ed.; Houghton Mifflin Company: Boston, MA, 1996.
(32) Mori, T.; Rezai-Zadeh, K.; Koyama, N.; Arendash, G. W.; Yamaguchi, H.; Kakuda, N.; Horikoshi-Sakuraba, Y.; Tan, J.; Town, T. *J. Biol. Chem.* **2012**, *287*, 6912−6927.
(33) Friedman, M.; Jurgens, H. S. *J. Agric. Food. Chem.* **2000**, *48*, 2101−2110.

(34) Choi, J.; Rubner, M. F. *Macromolecules* **2005**, *38*, 116−124.
(35) Sileika, T. S.; Barrett, D. G.; Zhang, R.; Lau, K. H. A.; Messersmith, P. B. *Angew. Chem., Int. Ed.* **2013**, *52*, 10766−10770.
(36) South, P. K.; Miller, D. D. *Food Chem.* **1998**, *63*, 167−172.
(37) Brune, M.; Hallberg, L.; Skanberg, A.-B. *J. Food Sci.* **1991**, *56*, 128−131.
(38) Hynes, M. J.; Coinceanainn, M. O. *J. Inorg. Biochem.* **2001**, *85*, 131−142.
(39) Chvátalováa, K.; Slaninováb, I.; Březinováa, L.; Slaninaa, J. *Food Chem.* **2008**, *106*, 650−660.
(40) Moulder, J. F.; Stickle, W. F.; Sobol, P. E.; Bomben, K. D. *Handbook of X-ray Photoelectron Spectroscopy*; Physical Electronics, Inc.: Chanhassen, MN, 1995.
(41) Gust, J.; Suwalski, J. *Corrosion* **1994**, *50*, 355−365.
(42) Zhou, Y.; Xing, X.-H.; Liu, Z.; Cui, L.; Yu, A.; Feng, Q.; Yang, H. *Chemosphere* **2008**, *72*, 290−298.
(43) Lopes, L.; de Laat, J.; Legube, B. *Inorg. Chem.* **2002**, *41*, 2505−2517.
(44) Sommer, B. A.; Margerum, D. W. *Inorg. Chem.* **1970**, *9*, 2517−2521.
(45) Bock, C. W.; Markham, G. D.; Katz, A. K.; Glusker, J. P. *Theor. Chem. Acc.* **2006**, *115*, 100−112.
(46) Kiwi, J.; Denisov, N.; Gak, Y.; Ovanesyan, N.; Buffat, P. A.; Suvorova, E.; Gostev, F.; Titov, A.; Sarkisov, O.; Albers, P.; Nadtochenko, V. *Langmuir* **2002**, *18*, 9054−9066.
(47) Caruso, F.; Caruso, R. A.; Möhwald, H. *Science* **1998**, *282*, 1111−1114.
(48) Donath, E.; Sukhorukov, G. B.; Caruso, F.; Davis, S. A.; Möhwald, H. *Angew. Chem., Int. Ed.* **1998**, *37*, 2201−2205.
(49) Caruso, F.; Möhwald, H. *J. Am. Chem. Soc.* **1999**, *121*, 6039−6046.
(50) Madhan, B.; Dhathathreyan, A.; Subramanian, V.; Ramasami, T. *Proc. Indian Acad. Sci. (Chem. Sci.)* **2003**, *115*, 751−766.
(51) Ariga, K.; Vinu, A.; Miyahara, M.; Hill, J. P.; Mori, T. *J. Am. Chem. Soc.* **2007**, *129*, 11022−11023.
(52) Radtchenko, I. L.; Sukhorukov, G. B.; Leporatti, S.; Khomutov, G. B.; Donath, E.; Möhwald, H. *J. Colloid Interface Sci.* **2000**, *230*, 272−280.
(53) Vinogradova, O. I.; Lebedeva, O. V.; Kim, B. S. *Annu. Rev. Mater. Res.* **2006**, *36*, 143−178.
(54) Sarhan, A. A. O.; Bolm, C. *Chem. Soc. Rev.* **2009**, *38*, 2730−2744.
(55) McBride, M. B.; Sikora, F. J. *J. Inorg. Biochem.* **1990**, *39*, 247−262.